

Correlations between 21 cm Radiation and the CMB from Active Sources

Aaron Berendsen^{1,2}, Levon Pogosian^{1,3} and Mark Wyman³

¹*Department of Physics, Simon Fraser University, Burnaby, BC, V5A 1S6, Canada.*

²*Department of Physics & Astronomy, University of British Columbia, Vancouver, BC, V6T 1Z1, Canada*

³*Perimeter Institute for Theoretical Physics, Waterloo, ON, L6H 2A4, Canada.*

(Dated: March 24, 2022)

Neutral hydrogen is ubiquitous, absorbing and emitting 21 cm radiation throughout much of the Universe’s history. Active sources of perturbations, such as cosmic strings, would generate simultaneous perturbations in the distribution of neutral hydrogen and in the Cosmic Microwave Background (CMB) radiation from recombination. Moving strings would create wakes leading to 21 cm brightness fluctuations, while also perturbing CMB light via the Gott-Kaiser-Stebbins effect. This would lead to spatial correlations between the 21 cm and CMB anisotropies. Passive sources, like inflationary perturbations, predict no cross correlations prior to the onset of reionization. Thus, observation of any cross correlation between CMB and 21 cm radiation from dark ages would constitute evidence for new physics. We calculate the cosmic string induced correlations between CMB and 21 cm and evaluate their observability.

I. INTRODUCTION

Neutral hydrogen emits and absorbs radiation at 21 cm in its rest frame throughout the history of the Universe. The brightness of the 21 cm line observed today from various redshifts is determined by the spatial distribution and peculiar velocity of the neutral hydrogen that emitted it. The radiation from any particular redshift has small angular variations, similar to those in the Cosmic Microwave Background (CMB) radiation. There is also variation along the line of sight, with a correlation depth of approximately 10 Mpc [1, 2]. In the absence of physics that violates free streaming, one does not expect a correlation among slices in the line-of-sight direction that are separated by more than this correlation length. Since observations can measure the redshift of 21 cm emission precisely, we should be able to extract information about this line of sight variation from 21 cm observations.

It is this third dimension of information encoded in 21 cm radiation that can make it a powerful new tool to learn about fundamental physics. One path forward is to look for physics that violates free streaming and generates correlations among distinct redshift shells [2]. Several sources of such a signal have been identified, though they are limited to the epoch during and after reionization [3–6]. Though passive perturbations, such as those seeded by inflation, cannot generate such correlations, active sources of perturbation could. Active sources of perturbation include cosmic strings and other topological defects, such as textures [7], as well as the field gradients that are left behind after global phase transitions [8]. Of these, cosmic strings are the most thoroughly studied and have perhaps the richest phenomenology [9], so they will be our focus.

Moving strings generate density wakes in the material through which they pass [10], including neutral hydrogen. As a result, the brightness of the 21 cm emission, which depends on the density and the velocity of the emitters, will be directly perturbed in the string’s wake [11]. The same moving strings also perturb the background CMB

light, monotonically shifting the spectra and creating line discontinuities in the temperature screen of the sky—a phenomenon known as the Gott-Kaiser-Stebbins (GKS) [12, 13] effect. GKS is a special case of the Integrated Sachs-Wolfe (ISW) effect [14] caused by time-varying gravitational potentials sourced by moving strings. Thus, there will be some correlation between string-sourced 21 cm brightness fluctuations at any redshift and a part of the CMB temperature anisotropy. Strings will also induce some cross-correlation in 21 cm fluctuations coming from different redshifts. However, as we discuss in Section II, we expect this effect to be relatively small.

Precision measurements of the CMB temperature anisotropy limit the contribution of cosmic string perturbations to be less than about 10% of the total over the range of scales covered by WMAP [15]. As such, the bulk of the Universe’s anisotropy comes from the primordial inflationary fluctuations, for which the cross-correlation between sufficiently-separated shells is zero. The fact that any string contribution to primordial anisotropy must be small means that the intrinsic signal for which we are searching will be faint. However, since there is nothing in the standard Λ CDM model that could generate such cross correlations before the epoch of reionization, we can be sure that discovery of such a cross correlation would be a sign of new physics.

To examine the prospects for detecting these string-induced correlations, we will evaluate the signal-to-noise density of this effect and the volume over which the signal can be found. Our aim is to identify the optimal way of looking for stringy phenomena in the 21 cm radiation from the dark ages. This effect is present over a vast volume—from $z \lesssim 100$ until the onset of reionization—which may make a detection of the CMB/21cm correlation feasible under optimistic observing scenarios. However, because of uncertainties in reionization physics, we exclude a large region ($z < 20$) from our present study. We will also leave the calculation of 21cm \times 21cm cross-correlation from different redshifts for future work.

In this paper we adopt the string network model of

[16, 17], which was previously implemented in CMBFAST [18] and made available publicly as CMBACT [19]. For this work, we have implemented this string model in CAMB [20]. Our code will be made publicly available soon [21].

II. 21 CM/CMB CORRELATION INDUCED BY COSMIC STRINGS

Cosmic strings are relativistically moving linear topological defects that are remnants of the high energy early Universe. As they move, strings affect matter by kicking it into over-dense wakes and perturb light by shifting its spectrum via the GKS effect. Strings form in the early Universe and remain active through all epochs, spreading their effects throughout the Universe’s history.

The effect of cosmic string networks on the CMB power spectrum has been well studied. Strings affect the CMB in both of the ways described above: their wakes generate a single peak at an angular scale determined by the strings’ correlation length ($\lesssim c/H$), and strings in the foreground of the CMB generate an interlacing network of linear discontinuities through the GKS effect. The fact that these signatures have not been observed provide a bound on the density and tension of cosmic strings [15].

These effects are also present during the dark ages, when the neutral hydrogen is releasing 21 cm radiation. Moving strings produce wakes and thus seed hydrogen density contrasts that grow and generate observable variations in the brightness temperature. Interestingly, though, the GKS effect is much less observable for 21 cm radiation. Strings shift the spectrum of light that passes them, so their effect on passing light is only observable when there is a noticeable change in the known background source, such as a shift in a spectral peak or discontinuity in a smoothly varying brightness. However, in the presence of a flat spectrum of background light, the string is invisible, since a lateral shift of a horizontal spectrum results in no detectable change. In the dark ages, strings will be swimming in a background of continuously renewed radio waves, with a very weak gradient in brightness and spectrum. Thus, the strings’ GKS effect on 21 cm radiation will be considerably less observable than the same effect applied to CMB photons¹.

To calculate these string-sourced effects quantitatively, we must give a formal characterization of the string perturbations. The most important difference between string-sourced perturbations and those from inflation, besides the active/passive distinction, is that strings source vector mode perturbations. For strings, vector modes are as large as scalar modes, and they also generate much of the novel phenomenology of string networks [22]. Vector modes are usually neglected since they decay in sys-

tems described by General Relativity and ordinary matter. Strings, however, actively source vector perturbations faster than they can decay away. We will reproduce the most relevant equations for vector mode perturbations in the Appendix.

Calculating CMB and 21 cm observables also requires a string model and a code for tracing the history of light streaming to us now from these early times. To this end, we have incorporated a model for strings [16, 17, 19] (see § IIA for a description) into the 21 cm extension of CAMB [20]; this code will be publicly released [21]. Our major addition to the underlying CAMB code is the inclusion of vector mode fluctuations. Details about how string-sourced vector modes enter the Boltzmann equation can be found in Refs. [16, 17, 20, 23], and will be more comprehensively explained in [21].

Now we can ask what physics will control the shape and amplitude of string-sourced two-point functions in the 21 cm fluctuations and in the cross correlation. The two physical effects controlling the shape of these spectra are 1) the intrinsic brightness of the 21 cm photons and 2) the correlation length of the string network. The brightness temperature sets the amplitude of the spectrum. It, in turn, is determined by the difference between the 21 cm spin temperature and the CMB temperature at that epoch, which are mismatched over a long period during the dark ages [2]. It is worth noting that the brightness temperature is negative throughout most of the dark ages. That is, the neutral hydrogen is absorbing, not emitting, radiation. This shows up as an observable because we can infer what the flux of long wavelength CMB photons should be, and hence detect the dimming due to neutral hydrogen. Since we are looking for small variations in the brightness temperature, a large intrinsic brightness makes detections easier. The anisotropy of 21 cm brightness is chiefly caused by variations in the density and the peculiar velocity of the neutral hydrogen, both of which are sourced by cosmic strings. These effects and others are more comprehensively discussed in Ref. [20].

The correlation length of the string network sets the location of the peak in ℓ -space, the angular scale. Since this correlation length is some fraction of the Hubble scale, the spectrum from dark ages strings peaks for multipoles $\ell < 100$. This peak in the two-point function corresponds to the size of the wakes generated by the string network at that epoch. Hence, the peak signal migrates to lower- ℓ as the redshift decreases since the network is scaling with the horizon, and the horizon is growing. This trend can be seen in our Fig. 1, a plot of the CMB-21 cm cross-correlation $C_\ell^{Tz}(z, \ell)$ from a string network, which we have generated with our code.

A. The string model

The string code we used is based on the segment model [16, 17]. In this model, the string network is represented

¹ We thank Mark Halpern for a discussion of this effect.

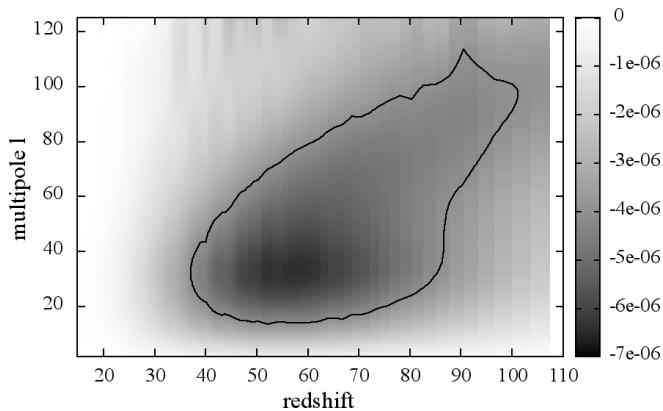


FIG. 1: CMB-21 cm cross-correlation power spectra ($C_\ell^{Tz} [\mu K]^2$) generated by a network of strings with tension $G\mu = 4 \times 10^{-7}$. The amplitude of the signal scales with the brightness temperature, peaking at a redshift $z \simeq 55$. The general shape—anti-correlation with a single broad peak—is similar for all redshifts, though the ℓ of maximum correlation moves to larger scales at later times / lower redshifts. This pattern comes from the string network’s scaling behaviour: strings seed fluctuations at a fixed fraction of the horizon size at the epoch in which the seed is created. This corresponds to larger scales (smaller ℓ ’s) for later times, i.e., for lower redshifts. A contour at $-4 \times 10^{-6} [\mu K]^2$ is shown.

by a collection of uncorrelated straight string segments moving with uncorrelated, random velocities. There are two fundamental length scales in such a model: ξ , the length of a string segment, which represents the typical length of roughly straight segments in a full network; and $\bar{\xi}$, the typical length between two string segments, which sets the number density of strings in a given volume ($N_s \propto 1/\bar{\xi}^2$). The model also tracks the root-mean-square (rms) velocity of the string segments. These parameters are deduced by assuming network scaling—i.e., the string energy density tracks the dominant background energy density in the radiation and matter eras. Numerical simulations of networks have confirmed that these assumptions accurately describe network physics. The positions and orientations of the segments are drawn from uniform distributions in space and on a two-sphere, respectively. The model’s parameters have been calibrated to produce source correlation functions in agreement with those in Ref. [24]. Because of the approximations built into the string segments, the model can only produce two-point correlation functions. It cannot be used for making simulated string maps or other more sophisticated observables; though it could, with some modification, generate three-point functions [25].

On the cosmological scales we consider, finer details of the string evolution do not play a major role. It is the large-scale properties—such as the scaling distance, the equation of state (wiggleness), and the rms velocity—that determine the shape of the string-induced spectra. Further details of the computational methods necessary to compute the 21 cm signal will be included in a subsequent

publication [21].

B. Cross correlations

Let $\delta T^z(\vec{x}, \hat{n})$ denote the anisotropy in the 21 cm brightness temperature emitted at redshift z and observed at a spatial position \vec{x} coming from the propagation direction \hat{n} . Similarly, the CMB brightness temperature is characterized by $\delta T^{CMB}(\vec{x}', \hat{n}')$. For computational purposes these quantities are expanded into normal modes [23]

$$\delta T^X(\vec{x}, \hat{n}) = \int \frac{d^3 \vec{k}}{(2\pi)^3} \sum_\ell \sum_{m=-2}^2 \delta T_{\ell m}^X(\vec{k}) G_\ell^m, \quad (1)$$

where \vec{k} is the Fourier conjugate to \vec{x} , $X \in \{z, \text{CMB}\}$ and $\delta T_{\ell m}^X$ are the associated multipole moments in the basis

$$G_\ell^m = (-i)^\ell \sqrt{\frac{4\pi}{2\ell+1}} Y_\ell^m(\hat{n}) \exp(i\vec{k} \cdot \vec{x}). \quad (2)$$

In our analysis we use the angular correlation function between quantities X and Y as measured by an observer at $\vec{x} = 0$, defined as

$$\begin{aligned} C^{XY}(\Theta) &\equiv \langle \delta T^z(\hat{n}) \delta T^{CMB}(\hat{n}') \rangle_{\hat{n} \cdot \hat{n}' = \cos \Theta} \\ &= \frac{1}{4\pi} \sum_{\ell=0}^{\infty} (2\ell+1) C_\ell^{XY} P_\ell(\cos \Theta) \end{aligned} \quad (3)$$

where P_ℓ are the Legendre polynomials, and C_ℓ^{XY} is the anisotropy spectrum calculated from the associated multipoles $\delta T^X(\vec{k})$ [18] [20] as

$$C_\ell^{XY} = (4\pi)^2 \int d^3 \vec{k} \sum_{m=-2}^2 \delta T_{\ell m}^X \delta T_{\ell m}^Y. \quad (4)$$

In the above notation, $m = 0$ corresponds to scalar modes, $m = \pm 1$ labels vector modes of right- and left-handed vorticity, and $m = \pm 2$ denotes the tensor modes. See the Appendix for an expanded discussion of our calculational method.

III. SOURCES OF NOISE

Having formed the cross correlation spectrum (Eq. (4)), a density distribution of signal-to-noise (S/N) can be formed in redshift and ℓ space as

$$\left(\frac{S}{N}\right)^2(z, \ell, \Delta z) = \frac{f_{\text{sky}}(2\ell+1) (C_\ell^{Tz})^2}{C_\ell^{TT} C_\ell^{zz} + (C_\ell^{Tz})^2}, \quad (5)$$

Δz is the width of the redshift shell set by the chosen frequency interval and $f_{\text{sky}} \simeq 0.8$ is the fraction of observable sky. The total signal-to-noise (S/N) is then

$$\left(\frac{S}{N}\right)_{\text{tot}}^2 = \sum_\ell \sum_{z_i} \left(\left(\frac{S}{N}\right)^2(z_i, \ell, \Delta z_i) \right), \quad (6)$$

where the sum is over the harmonic multipoles ℓ and the (independent) observed redshift slices z_i of width Δz_i , determined by the observational setup. Each multipole can receive contributions from the inflationary background C_ℓ^{ad} , the active sources C_ℓ^{str} , and astrophysical and telescope noise C_ℓ^N , so we can write

$$C_\ell^{XY}[\text{total}] = C_\ell^{adXY} + C_\ell^{strXY} + C_\ell^NXY. \quad (7)$$

Strings are the only source of the cross-correlation, so the numerator in Eq. (5) receives only one contribution. The denominator, however, receives a large contribution from inflationary perturbations that are at least ten times the size of the string power spectrum. There is also a large contribution from the detector noise which is dominated by the galactic emission at the low frequencies we need to probe the high redshift 21 cm brightness temperature. The detector noise is uncorrelated between the CMB and 21 cm frequencies and is given by

$$C_\ell^N = \frac{(2\pi)^3 T_{\text{sys}}^2(\nu)}{\Delta\nu t_{\text{obs}} f_{\text{cover}}^2 \ell_{\text{max}}^2(\nu)}, \quad (8)$$

where T_{sys} is dominated by the sky temperature and, for regions away from the galactic plane, can be approximated as [2]

$$T_{\text{sys}}(\nu) = 150\text{K} \left(\frac{\nu}{180\text{MHz}} \right)^{-2.6}. \quad (9)$$

In the previous expressions $\Delta\nu$ is the width of a frequency bin, which is set by the experiment, t_{obs} is the observing time, $f_{\text{cover}} \equiv N_{\text{dish}} A_{\text{dish}} / A_{\text{total}}$ is the fraction of the total area enclosed by the experiment and characterizes the total collecting area, and $\ell_{\text{max}}(\nu) = 2\pi D_{\text{array}} \nu / c$, where D_{array} is the diameter of the array and c is the speed of light.

Foregrounds include galactic and extragalactic point sources, as well as the galactic and extragalactic free-free emission, all of which are expected to induce correlations between different frequencies [26, 27]. In this study, however, astrophysical sources will have a negligible effect since we are only including 21 cm cross-correlations with CMB photons, and these signals quickly decorrelate with increasing frequency separation [2]. Furthermore, these signals dominate on very small scales while string-induced correlations reside on large scales, $\ell \lesssim 100$.

We fold the observational parameters into a single observational ambition parameter, x , defined as

$$x \equiv t_{\text{obs}} f_{\text{cover}}^2 D^2, \quad (10)$$

with units of $[x] = [\text{years}] \times [\text{km}]^2$. There is always a practical trade-off between making f_{cover} large and making D large. For our signal, though, it is clear what we should choose. The main reason for going to large D is to resolve very small angular scales. However, string sourced cross correlations reside only on large angular scales. Hence, we can make due with a relatively small baseline D , which should let us make f_{cover} nearly unity; i.e., a “moderately” sized telescope or array with nearly a complete covering area would be ideal for searching for strings.

IV. RESULTS

We have calculated cross correlation power spectra from redshifts throughout the dark ages. In producing our results, we have fixed the observing bandwidth to $\Delta\nu = 0.5\text{MHz}$; however, varying this does not change our result. Although increasing the bandwidth diminishes the autocorrelator signal (noise “ N ” $\propto 1/\Delta\nu$) and, thus, increases the signal-to-noise in each redshift bin, one observes fewer independent redshift slices as a result (signal “ S_{tot} ” $\propto 1/\Delta\nu$) so the overall signal-to-noise remains unchanged to first order. We have numerically verified this for bandwidths in the range $0.01\text{MHz} < \Delta\nu < 2\text{MHz}$.

We have excluded the epoch of reionization ($z < 20$) from our signal-to-noise results. There are several reasons for this. The main reason is that reionization physics are still too uncertain for reliable calculations to be done, and the details of reionization, once begun, will dominate the 21 cm physics. Moreover, if cosmic strings are present during reionization, they will likely play a role in speeding up the process of reionization through their early generation of non-linear overdensities [28, 29]. Reionization itself will also create cross-correlations between the CMB and 21 cm radiation [3–6]. Though it is possible that the string and reionization signals could be disentangled if they are both present, we restrict ourselves in the present study to redshifts where strings are the only possible source of cross-correlation.

At redshifts $z \lesssim 7$ reionization is complete and the surviving neutral hydrogen only exist in islands that are presumably correlated with large scale structure. In principle, we can continue calculating the string sourced cross correlation between the matter distribution (traced via 21 cm or any other observable light) and the CMB. However, there will be competing sources of cross correlation. For instance, the re-scattering of CMB photons off ionized particles will induce a correlation of CMB with the large-scale plasma distribution [30]. Eventually, at lower redshifts, there will be a correlation between large scale structure and the ISW distortion of the CMB caused time varying potentials when Dark Energy becomes dynamically important. Nonetheless, we have made an approximate calculation of what a hypothetical radio survey at these redshifts might see in the presence of strings, extending an analytical distribution of large scale structure tracers used in [31] to the range $0 < z < 7$. The resulting theoretical signal-to-noise for the cross correlation was too small. This is not surprising since string wakes that are sourced at such late times have not had time to grow. By contrast, the potential wells that attract the ionized particles which then re-scatter CMB have been growing through gravitational instability for some time since entering the horizon. Hence, we do not include the $z \leq 7$ range into our signal-to-noise results.

Let us turn to our results, shown in Fig. 2, which begin with analysis of a hypothetical Universe where inflationary perturbations are not present and cosmic strings are the only source of both CMB and 21 cm anisotropy. We

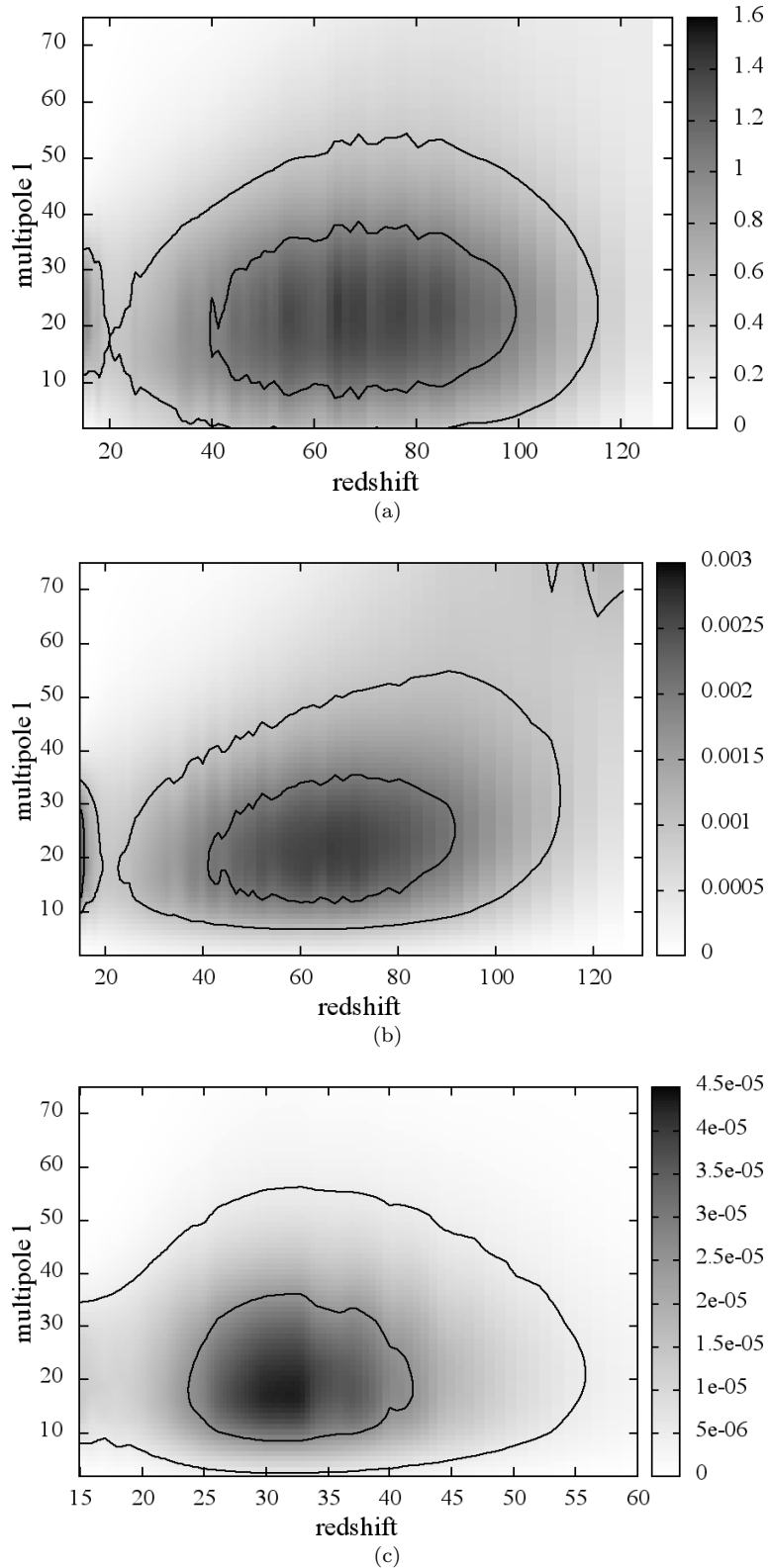


FIG. 2: Distribution of signal-to-noise squared $(S/N)^2$ from cross-correlation studies between CMB and 21 cm photons in the presence of a string network. The observing bandwidth has been fixed to $\Delta\nu = 0.5\text{MHz}$, which determines the redshift bin width $|\Delta z| = (1+z)^2 \Delta\nu/\nu_0$, ν_0 being the rest frequency of the 21 cm radiation. Signal along horizontal slices is modulated by the brightness temperature, which nulls around the epoch of first light as the HI regions transit from absorption to emission. Signal along vertical slices is set by the correlation length of the network, a fraction of the Hubble scale. Fig. 2(a) shows an idealized situation where structure is seeded only by strings, in the absence of foreground noise. Contours of 0.5 and 1.0 are shown. In Figs. 2(b), 2(c), $G\mu = 4 \times 10^{-7}$, representing a system primarily seeded by inflation, but with a 10% contribution from strings. Fig. 2(b) includes no sky noise, and has contours representing 0.001 and 0.002. Fig. 2(c) includes noise, and assumes ten year's observation from a square kilometre array ($D = 1\text{km}$, $x = 10$); recall that $x \equiv t_{\text{obs}} f_{\text{cover}}^2 D^2$. Contours of 5×10^{-6} and 2.5×10^{-6} are shown. These plots primarily serve to indicate where signal resides in the observing volume.

plot the cross correlation signal-to-noise distribution for this case in Fig. 2(a). When only strings are present and noise is disregarded, as we do here, the overall normalization, the string tension $G\mu$, drops out of the signal-to-noise calculation. In this imaginary Universe, the signal is so strong that an observation at each redshift would generate a detection ($(S/N)(z, \ell, \Delta z) > 1$).

In the real Universe, the inflationary perturbations overwhelm those from strings, as we see in Fig. 2(b), even without including the detector noise. No single measurement now has significant signal-to-noise ($(S/N) > 1$). Instead, we must sum over many independent redshift bins in order to accumulate a significant signal, giving a statistical detection. The case presented in this figure represents the best-case scenario: no noise and a maximal, ten percent contribution to primordial anisotropy from strings. The signal is similar in shape to, though lower in magnitude than, the idealized case of a system seeded only by strings. The signal is suppressed more significantly on small angular scales, since the inflationary auto-correlations monotonically increases for ℓ , while the string-induced signal peaks at $\ell \simeq 60$. Although any particular observation in the $z - \ell$ plane will result in a contribution $(S/N)^2 \simeq \mathcal{O}(10^{-3})$, the statistical benefit of observing roughly 50 multipoles ($2 < \ell < 50$, weighted by a factor of $2\ell + 1$) in roughly 50 redshift bins (observations with a 1MHz bandwidth in the range $20 < z < 120$) gives rise to a total $(S/N) \simeq \sqrt{(50)^3 10^{-3}} \simeq \mathcal{O}(10)$. Summing our simulated data over all ℓ and over $70 \leq z \leq 20$ reveals a $(S/N) \simeq 3$. However, this does not include experimental noise, and corresponds to a survey-strategy parameter of $x = \infty$.

Fig. 2(c) shows the remaining signal once the sky temperature is incorporated. These data were generated assuming an all-sky survey from a single dish of diameter 1km observing for ten years ($x = 10$); note that sky temperature completely overwhelms the signal for redshift $z > 50$. The estimated signal-to-noise remaining in our analysis volume is $(S/N) \simeq 0.28$.

V. OBSERVATIONAL OUTLOOK

Finally, let us look at Fig. 3, which summarizes the detectability of our signal for various string tensions, $G\mu$, as a function of our observational parameter, x . It is clear that the noise induced by the large sky temperatures severely limits the possibility of observing a string network through cross-correlation. However, the calculation reported here does not exhaust the possible locations of cross-correlation signal from strings. For instance, our estimate is restricted to the domain $z > 20$ that we are certain will not be affected by reionization. Our present ignorance about the physics of reionization means that we cannot trust our calculation into the $z < 20$ range. This is a major impediment, though: lower z is the redshift range least affected by noise, since noise goes as an inverse power law with frequency. Hence, we can hope to

boost our signal significantly once the physics of reionization are better understood.

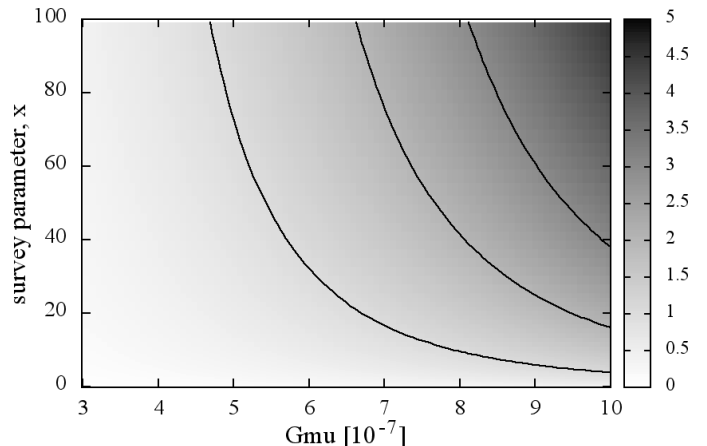


FIG. 3: Signal-to-noise as a function of observing strategy (represented by $x \equiv t_{\text{obs}} f_{\text{cover}}^2 D^2$, in units of years \times km²) and the string tension $G\mu$. Contours of $S/N = 1, 2$, and 3 are shown.

We have also only looked at the CMB-21 cm cross-correlations in this study. Although they are likely very small, we are currently analyzing contributions from the $\mathcal{O}(10^3)$ 21 cm-21 cm cross-correlations. These will also give some boost to our signal.

VI. DISCUSSION

By incorporating the segment model of strings into the CAMB_sources Einstein-Boltzmann code, we have calculated the cross correlation between the 21 cm brightness temperature and the CMB. Our chief result is plotted in Fig. 3, which represents the signal-to-noise available in CMB-21 cm correlation studies given an all-sky survey, a string tension $G\mu$, and our observing strategy, which we characterize by a single integration time and telescope properties parameter, x . Unfortunately, noise from the sky temperature overwhelms the signal we are calculating for observationally-allowed cosmic string tensions.

However, there is room for more work. We have thus far only included the signal from the CMB-21 cm correlations for $z > 20$, where we do not need to know the physics of reionization. Since the signal should extend until the epoch of reionization $z \simeq 10$, we may eventually be able to include $\mathcal{O}(10^2)$ more redshift bins and $\mathcal{O}(10^3)$ data points in the $z - \ell$ plane, once we can accurately model reionization. Another contribution to our signal that was neglected in this study can be found from a cross-correlation study between different redshift bins, and this signal will be addressed in future work [21]. It is possible that we will find a detectable signal when these extra sources of data are included in the analysis.

Though our calculations have not predicted a detectable signal, we reiterate that any detection of a cross

correlation between the 21 cm radiation from $z > 20$ and the CMB would be a clear sign of new physics. Active sources, such as cosmic strings, are a promising candidate for the sort of new physics that could generate this correlation. However, the fact that inflation very likely provides the dominant source of perturbations in the Universe makes detectability of any signal difficult: the inflationary perturbations must necessarily enter as “noise” for any study like this, and are typically much larger than any alternate sources of perturbation, at least prior to recombination where measurements of the CMB limit any non-inflationary perturbations. One way around this would be to contrive some active source that was suppressed prior to recombination which subsequently sourced a larger fraction of perturbations in the dark ages. On the other hand, a non-detection of such a cross correlation would constitute a strong constraint on active sources with such unusual properties.

Acknowledgments

A.B. is supported by the National Sciences and Engineering Research Council of Canada (NSERC) National Postdoctoral Fellowship. L.P. is supported by an NSERC Discovery grant. The work of M.W. at the Perimeter Institute is supported by the Government of Canada through Industry Canada and by the Province of Ontario through the Ministry of Research & Innovation.

Appendix A: 21 cm vector modes

In the absence of active sources vector perturbations quickly decay and, for that reason, are frequently ignored.

In particular, they are not included in the 21 cm extension to CAMB [20]. Cosmic strings, however, actively source vector modes and provide a significant contribution to CMB and 21 cm anisotropies. A large effort was spent incorporating their effects into our numerical code [21], and we elaborate on some of the details here.

Applying the harmonic decomposition described in [23] and Eq. (2) to (fluctuations in) the photon distribution f provided in [20] gives scalar $m = 0$, vector $m = \pm 1$ and tensor $m = \pm 2$ contributions to the expanded field:

$$\delta f(\eta, \vec{x}, \epsilon, \hat{n}) = \int \frac{d^3 \vec{k}}{(2\pi)^3} \sum_{l,m} F_l^{(m)}(\eta, \epsilon, \vec{k}) {}_0G_l^m. \quad (\text{A1})$$

The photon fluid is characterized at some conformal time η and position \vec{x} as photons coming from some direction \hat{n} with an energy $\epsilon = a(\eta)E_{21}$. The quantity ϵ represents the Doppler shifted energy of a 21 cm photon, E_{21} , stretched by the scale factor $a(\eta)$. \vec{k} is the Fourier conjugate to the spatial coordinate \vec{x} , we denote $k = |\vec{k}|$.

Expressions for the harmonic multipoles $F_l^{(m)}$ are formally obtained by integrating the Boltzmann equation for 21 cm photons along the line of sight [18]. The scalar contribution $F_l^{(0)}$ has been reported in [20], while for vector modes we find

$$\begin{aligned} F_l^{(1)}(\eta_A, \epsilon, \vec{k}) &\simeq -e^{-\tau_c} \bar{f}(\epsilon) \frac{r_\tau}{\mathcal{H}} v^{(1)} \left(\frac{j_l'(k\chi_\epsilon)}{\chi_\epsilon} - \frac{j_l(k\chi_\epsilon)}{k\chi_\epsilon^2} \right) + \int_{\eta_c}^{\eta_A} d\eta \dot{\tau}_c e^{-\tau_c} \bar{f}_{,\ln \epsilon}(\epsilon) v^{(1)} \frac{j_l(k\chi)}{k\chi} \\ &- e^{-\tau_c} \left\{ \bar{f}(\epsilon) \cdot \left[v^{(1)} + \frac{\bar{T}_\gamma}{\bar{T}_s - \bar{T}_\gamma} (v_\gamma^{(1)} - v^{(1)}) + \frac{r_\tau}{\mathcal{H}} \dot{v}^{(1)} + (r_\tau - 1)v^{(1)} \right] + \bar{f}_{,\ln \epsilon}(\epsilon) v^{(1)} \right\} \frac{j_l(k\chi_\epsilon)}{k\chi_\epsilon} \\ &- e^{-\tau_c} \bar{f}(\epsilon) \frac{\bar{T}_\gamma}{\bar{T}_s - \bar{T}_\gamma} \sum_{l'=2}^{\infty} \Theta_{l'} P_{l'} \left(\frac{-i}{k} \frac{d}{d\chi_\epsilon} \right) j_l(k\chi_\epsilon) + \int_{\eta_c}^{\eta_A} d\eta \dot{\tau}_c e^{-\tau_c} \bar{f}_{,\ln \epsilon}(\epsilon) \frac{\sqrt{3} F_2}{4} \left(\frac{j_l'(k\chi_\epsilon)}{\chi_\epsilon} - \frac{j_l(k\chi_\epsilon)}{k\chi_\epsilon^2} \right) \end{aligned} \quad (\text{A2})$$

for $l \geq 1$, where a prime denotes a derivatives with respect to the argument and a bar denotes a background value. Here, τ_c is the Thomson scattering optical depth, τ_ϵ is the optical depth to 21 cm radiation, $v^{(1)}$ is the vector component to the baryon velocity, $v_\gamma^{(1)}$ is the velocity (dipole) of the photon distribution, \bar{f} is the background photon distribution function, \bar{T}_γ is the photon temperature, \bar{T}_s is the spin-flip temperature of the neutral hydro-

gen and determines how much the hydrogen is emitting, $r_\tau \equiv \tau_c e^{-\tau_c} / (1 - e^{-\tau_c})$, \mathcal{H} is the conformal Hubble parameter, $\chi_\epsilon \equiv \eta_A - \eta_c$ is the conformal distance along the line of sight, and $j_l(k\chi_\epsilon)$ is the spherical Bessel function. Quantities subscripted with ϵ are evaluated at the conformal time η_c . The Θ_ℓ are the angular moments of the Fourier expansion of the CMB temperature anisotropy. All quantities are discussed at length in [20].

The 21 cm power spectra referenced in the main text were given in terms of the brightness temperature T_b . This relates to the photon distribution function f through the relation

$$T_b = \frac{E_{\text{obs}} h_p^3 f}{2k_b} \quad (\text{A3})$$

where E_{obs} is the observed frequency of the 21 cm emis-

sion, h_p is the Planck constant, and k_b is the Boltzmann constant. Thus, anisotropies in the 21 cm brightness temperature emitted at a redshift z are given as

$$\delta T^z(\vec{x}, \hat{n}) = \frac{E_{\text{obs}} h_p^3}{2k_b} \delta f(\eta, \vec{x}, \epsilon, \hat{n}). \quad (\text{A4})$$

-
- [1] D. J. Eisenstein *et al.* [SDSS Collaboration], *Astrophys. J.* **633**, 560 (2005) [arXiv:astro-ph/0501171].
- [2] S. Furlanetto, S. P. Oh and F. Briggs, *Phys. Rept.* **433**, 181 (2006) [arXiv:astro-ph/0608032].
- [3] M. A. Alvarez, E. Komatsu, O. Dore and P. R. Shapiro, *Astrophys. J.* **647**, 840 (2006) [arXiv:astro-ph/0512010].
- [4] A. Slosar, A. Cooray and J. Silk, *Mon. Not. Roy. Astron. Soc.* **377**, 168 (2007) [arXiv:astro-ph/0701571];
- [5] P. Adshead and S. Furlanetto, arXiv:0706.3220 [astro-ph];
- [6] T. G. Sarkar, K. K. Datta and S. Bharadwaj, *JCAP* **0908**, 019 (2009) [arXiv:0810.3649 [astro-ph]].
- [7] N. Turok, *Phys. Rev. Lett.* **63**, 2625 (1989).
- [8] K. Jones-Smith, L. M. Krauss and H. Mathur, *Phys. Rev. Lett.* **100**, 131302 (2008) [arXiv:0712.0778 [astro-ph]].
- [9] R. C. Myers and M. Wyman, "Cosmic superstrings," *In *Erdmenger, J. (ed.): String cosmology* 121-156* (2009)
- [10] A. Vilenkin, *Phys. Rev. Lett.* **46**, 1169 (1981) [Erratum-ibid. **46**, 1496 (1981)];
Y. B. Zeldovich, *Mon. Not. Roy. Astron. Soc.* **192**, 663 (1980).
- [11] R. Khatri and B. D. Wandelt, *Phys. Rev. Lett.* **100**, 091302 (2008) [arXiv:0801.4406 [astro-ph]].
- [12] J. R. Gott III, *Astrophys. J.* **288**, 422 (1985).
- [13] N. Kaiser and A. Stebbins, *Nature (London)* **310**, 391 (1984).
- [14] R. K. Sachs and A. M. Wolfe, *Astrophys. J.* **147**, 73 (1967) [*Gen. Rel. Grav.* **39**, 1929 (2007)].
- [15] M. Wyman, L. Pogosian and I. Wasserman, *Phys. Rev. D* **72**, 023513 (2005) [Erratum-ibid. *D* **73**, 089905 (2006)] [arXiv:astro-ph/0503364];
M. Landriau and E. P. S. Shellard, *Phys. Rev. D* **69** 023003 (2004), astro-ph/0302166;
L. Pogosian, M. Wyman and I. Wasserman, *JCAP* **09** (2004) 008, astro-ph/0403268;
N. Bevis, M. Hindmarsh, M. Kunz and J. Urrestilla, *Phys. Rev. Lett.* **100**, 021301 (2008) [arXiv:astro-ph/0702223];
- R. A. Battye, B. Garbrecht, A. Moss and H. Stoica, *JCAP* **0801**, 020 (2008) [arXiv:0710.1541 [astro-ph]].
- [16] L. Pogosian and T. Vachaspati, *Phys. Rev. D* **60**, 083504 (1999) [arXiv:astro-ph/9903361]; L. Pogosian, I. Wasserman and M. Wyman, arXiv:astro-ph/0604141.
- [17] A. Albrecht, R. A. Battye and J. Robinson, *Phys. Rev. Lett.* **79**, 4736 (1997); *Phys. Rev.* **D59**, 023508 (1999).
- [18] U. Seljak and M. Zaldarriaga, *Astrophys. J.* **469**, 437 (1996) [arXiv:astro-ph/9603033].
- [19] <http://www.sfu.ca/~levon/cmbact.html>
- [20] A. Lewis, A. Challinor and A. Lasenby, *Astrophys. J.* **538**, 473 (2000) [arXiv:astro-ph/9911177]; A. Lewis and A. Challinor, *Phys. Rev. D* **76**, 083005 (2007) [arXiv:astro-ph/0702600].
- [21] A. Berndsen and L. Pogosian, *in preparation*.
- [22] L. Pogosian, I. Wasserman and M. Wyman, arXiv:astro-ph/0604141;
L. Pogosian and M. Wyman, *Phys. Rev. D* **77**, 083509 (2008) [arXiv:0711.0747 [astro-ph]].
- [23] W. Hu and M. J. White, *Phys. Rev. D* **56**, 596 (1997) [arXiv:astro-ph/9702170].
- [24] G. R. Vincent, M. Hindmarsh and M. Sakellariadou, *Phys. Rev. D* **55**, 573 (1997) [arXiv:astro-ph/9606137].
- [25] A. Gangui, L. Pogosian and S. Winitzki, *Phys. Rev. D* **64**, 043001 (2001) [arXiv:astro-ph/0101453].
- [26] M. Zaldarriaga, S. R. Furlanetto and L. Hernquist, *Astrophys. J.* **608**, 622 (2004) [arXiv:astro-ph/0311514].
- [27] M. G. Santos, A. Cooray and L. Knox, *Astrophys. J.* **625**, 575 (2005) [arXiv:astro-ph/0408515].
- [28] M. J. Rees, *MNRAS* **222**, 27 (1986)
- [29] L. Pogosian and A. Vilenkin, *Phys. Rev. D* **70**, 063523 (2004) [arXiv:astro-ph/0405606].
- [30] T. Giannantonio and R. Crittenden, *Mon. Not. Roy. Astron. Soc.* **381**, 819 (2007) [arXiv:0706.0274 [astro-ph]].
- [31] W. Hu and R. Scranton, *Phys. Rev. D* **70**, 123002 (2004) [arXiv:astro-ph/0408456].